Computers and Geotechnics 100 (2018) 15–29

Contents lists available at ScienceDirect

Computers and Geotechnics

journal homepage: www.elsevier.com/locate/compgeo

Research Paper

Numerical simulation of two-tier geosynthetic-reinforced-soil walls using two-phase approach

Ehsan Seyedi Hosseininia[a,*], Ahoo Ashjaee[b]

[a] Civil Engineering Department, Faculty of Engineering, Ferdowsi University of Mashhad, Iran
[b] Civil Engineering Department, Mazandaran Institute of Technology, Iran

ARTICLE INFO

Keywords:
Reinforced soil
Two-tier walls
Two-phase model
Numerical simulation
Deformation
Performance

ABSTRACT

In this study, the mechanical behavior of two-tier Geosynthetic-Reinforced Soil walls is investigated numerically by using the concept of two-phase systems. Comparison of the results of this approach with those of discrete numerical models and centrifuge tests indicates that the approach has the ability to consider the interaction between tiers, predict the reinforcement load and wall-face displacement. Furthermore, it is more cost-effective. The limitations of this approach pertain to the prediction of the failure surface and the wall deformation regime. Totally, the two-phase approach can be properly applied in a fast, effective and safe manner.

1. Introduction

Geosynthetic-Reinforced Soil (GRS) walls are now widely used in civil engineering practice. In some cases, GRS walls are designed and constructed in tier configurations rather than utilizing them as single walls due to wall stability, construction constraints, space requirements for drainage along the height of the wall, and aesthetics. The wall design with tier configuration is more complicated than a single wall since the upper and lower tiers mutually interact over wall deformation and reinforcement loads.

There are generally two approaches for design and analysis of multi-tier GRS walls. A lateral earth pressure method, which is based on an empirical extension of single-tier GRS walls, is introduced by the NCMA [1] and FHWA guidelines [2,3]. This method results in an overestimation of design requirements [4–8]. The limit equilibrium (LE) method whose applicability has been examined and approved in [4,5,9,10] is another approach. These two approaches are only yield wall stability and no information about wall deformation and reinforcement load distribution can be obtained. Thus, numerical analyses should be implemented in the design procedure.

Numerical methods have been widely used in order to study the performance of multi-tier GRS walls as well as the interactions between the tiers. Yoo and Song [11] performed plane-strain finite element simulation of two-tier GRS segmental retaining walls. The results indicate that an unexpected yield in the foundation may affect both internal and external stability of the lower tier owing to the absence of toe resistance. In addition, upper-tier reinforcement length has a significant influence on lower-tier lateral deformation. Yoo and Kim [12] calibrated a three-dimensional finite element (FE) model of a full-scale test wall to further investigate load carrying capacity and relevant performance of the test wall under surcharge load. Stuedlein et al. [9] simulated a four-tier 46-m-tall reinforced wall using the finite difference code FLAC. Although the overall design in this work was based on the LE method, they utilized numerical simulations in order to assess wall performance and predict wall displacements at times of soil liquefaction. Yoo et al. [8] carried out a series of finite element (FE) analyses in order to investigate internal stability of small-scale two-tier GRS walls with various offset distances and reinforcement distributions. They showed that the lower-tier reinforcement length has a greater effect on overall wall stability than the upper-tier reinforcement length. Recently, Mohamed et al. [6] compared the results of numerical simulations of two-tier GRS walls with those of a centrifuge modeling series which included different offset distances. They concluded that there is an excellent agreement for slip surfaces and reinforcement loads between the LE/FE methods and centrifuge tests. Generally, it can be said that in comparison with the LE method, numerical methods offer more comprehensive information about stress, strain, force, and displacement at any location of interest.

We can consider the reinforced soil medium as a composite which behaves, at the macroscopic level, as a homogenous but anisotropic composite material [e.g. 13–16] due to the existence of repeated layers of soil and reinforcing elements in a periodic manner. For reinforced soil medium, a new concept called the "Multiphase Model" has been introduced by de Buhan and Sudret [17] which is an extension of the

* Corresponding author.
E-mail addresses: eseyedi@um.ac.ir (E. Seyedi Hosseininia), ashjaee.a@gmail.com (A. Ashjaee).

https://doi.org/10.1016/j.compgeo.2018.04.003
Received 9 October 2017; Received in revised form 28 February 2018; Accepted 2 April 2018

classical homogenization technique. In this technique, the composite is represented at the macroscopic scale not by a single medium as in the homogenization methods, but by superposed mutually interacting media (or "phases"). Accordingly, reinforced soil can be regarded as a two-phase medium such that each geometrical point represents two coincident particles including matrix phase (representative of soil) and reinforcement phase (representative of inclusions). In general, it is possible to dedicate different kinematic fields to each phase relating to each other through an interaction law. Consequently, the multiphase model can capture both scale and boundary effects [18] contrary to classical homogenization methods. The two-phase model has been utilized in order to investigate the performance of single GRS walls under static [19–21] and dynamic loads [22].

The mechanical behavior of two-tier GRS walls is investigated by using the two-phase approach and numerical simulations in the present study. The numerical finite difference method is used in this work. The applicability of the two-phase approach to consider tiers interaction and the influence of gird size are investigated. The results are compared with those of centrifuge modeling performed by Mohamed et al. [5]. For simplicity, the Mohr-Coulomb model is selected for the soil constitutive model and a linear elastic perfectly-plastic model is considered for reinforcements. The discrete modeling approach is also utilized in this study to get a better understanding of the capability of the two-phase approach.

2. Reinforced soil as a two-phase material

Fig. 1 presents the concept of a two-phase material for reinforced soil. According to Fig. 1a, reinforced soil is a periodic medium in which reinforcement layers are placed in a systematic order among the soil medium. A two-phase system introduces a macroscopic description of a composite medium as superposition of two individual continuous media called phases. Each point of the geometry in a two-phase material consists of matrix phase that represents soil and reinforcement phase implying axial inclusions as shown in Fig. 1b. The two-phase concept has also been implemented to simulate the behavior of reinforced soil structures. In such structures, linear elements such as piles or bolts are installed in the soil in order to augment the bearing capacity or reduce the deformations of the soil medium. Examples of two-phase problems of reinforced soil structures are using bolts in tunneling [23,24], piled rafts [25–27], and piled embankments [28].

In a two-phase material, each phase has its own specific characteristics similar to what is defined for each constituent in discrete form. Based on the theory of the virtual work method, the equilibrium equation for each phase is defined separately as follows [17,29]:

$$div\boldsymbol{\sigma}^m + \rho^m\mathbf{F}^m + \mathbf{I} = \mathbf{0} \tag{1}$$

for the matrix phase, and

$$div\boldsymbol{\sigma}^r + \rho^r\mathbf{F}^r - \mathbf{I} = \mathbf{0} \tag{2}$$

for the reinforcement phase. The bold face letters in the equations are denoted as tensors and vectors. In the above equations, the superscripts m and r correspond to the matrix and reinforcement phases, respectively. $\boldsymbol{\sigma}$ denotes the stress tensor of each phase. The term $\rho\mathbf{F}$ indicates the external (body) force vector applied to the phases and $\mathbf{I}$ represents the interaction force vector mutually exerted from the phases. These equilibrium equations will be completed by the corresponding stress boundary conditions that are prescribed on the boundary surface of each phase separately.

The summation in Eqs. (1) and (2) gives the global equilibrium equation of a two-phase material in the following form

$$div\sum + \rho\mathbf{F} = \mathbf{0} \tag{3}$$

where

$$\sum = \boldsymbol{\sigma}^m + \boldsymbol{\sigma}^r, \quad \rho\mathbf{F} = \rho\mathbf{F}^m + \rho\mathbf{F}^r \tag{4}$$

$\sum$ represents the global stress tensor of a two-phase material which is the sum of partial stresses of both phases. Similarly, $\rho\mathbf{F}$ indicates the global body force of the two-phase material.

In a two-phase material, each phase has its own domain of kinematics which are defined by strain tensors $\boldsymbol{\varepsilon}^m$ and $\boldsymbol{\varepsilon}^r$ for matrix and reinforcement phases, respectively. For each phase, the stress-strain relationship is introduced individually:

$$\boldsymbol{\sigma}^m = \mathbf{D}^m\boldsymbol{\varepsilon}^m, \quad \boldsymbol{\sigma}^r = \mathbf{D}^r\boldsymbol{\varepsilon}^r \tag{5}$$

where $\mathbf{D}^m (or\ \mathbf{D}^r)$ denotes the stiffness tensor of the matrix (or reinforcement) phase. The interaction body force $\mathbf{I}$ in Eqs. (1) and (2) can be defined as a function of relative displacement between phases [e.g. 20, 30, 31]. In the case of perfect bonding between phases, the kinematics of the phases become identical:

$$\in = \boldsymbol{\varepsilon}^m = \boldsymbol{\varepsilon}^r \tag{6}$$

where $\in$ denotes the strain tensor of the whole medium.

By considering Eqs. (4) and (6), the global stress-strain relationship of a two-phase material in the case of perfect bonding has the following tensor form:

$$\boldsymbol{\Sigma} = \mathbf{D}\in \tag{7}$$

where $\mathbf{D} = \mathbf{D}^m + \mathbf{D}^r$ and indicates the global stiffness tensor of the two-phase material.

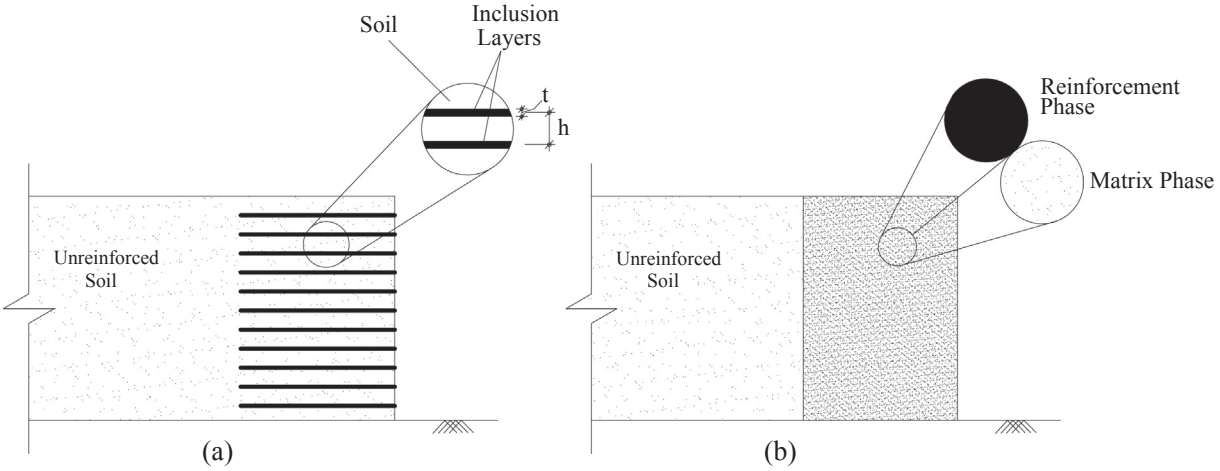

Fig. 1. Schematics of a reinforced soil wall: (a) in discrete form; (b) as a two-phase material.

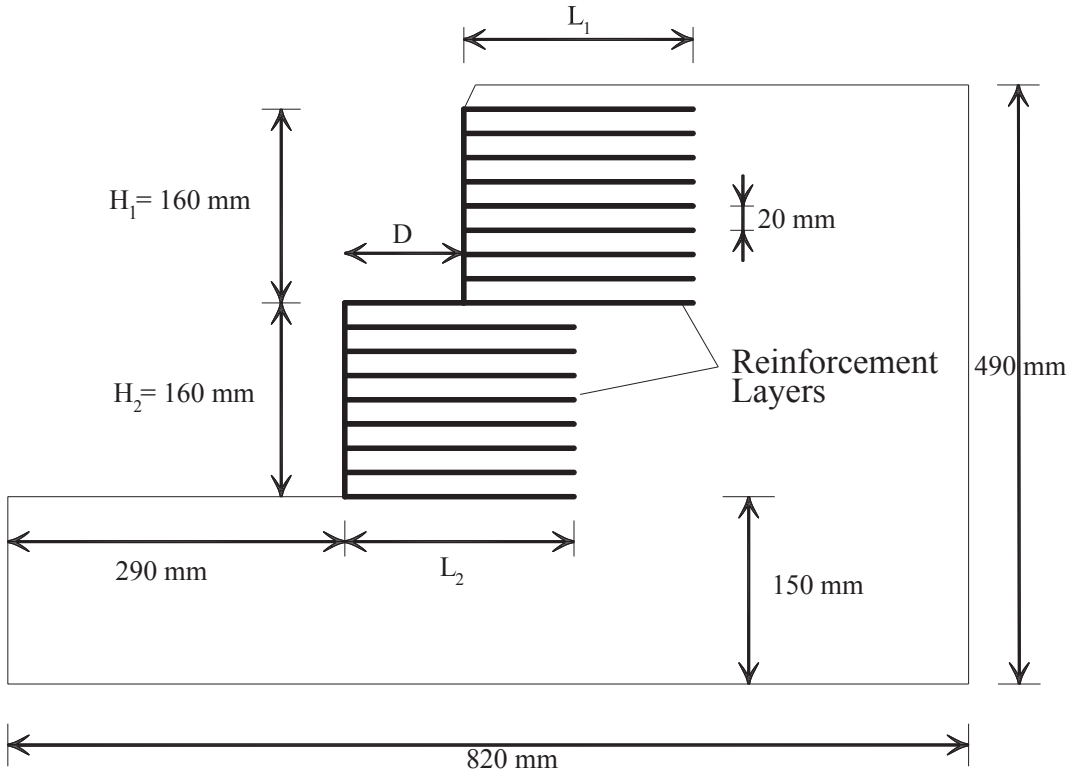

Fig. 2. Presentation of the geometry of the model walls used in the centrifuge tests performed by Mohamed et al. [6].

Table 1
Wall geometrical configurations used in the centrifuge tests.

Wall type	Single	Compound[a]				Independent
Label	S1	C4	C6	C9	C10	I11
D (mm)	Zero	30	50	80	90	260
L_1 (mm)	224	192	192	192	192	112
L_2 (mm)	224	192	192	192	192	112

[a] According to FHWA: 17 mm < D < 176 mm (for ϕ = 42.3°).

2.1. Reinforcement phase behavior

In this study, reinforcing inclusions are considered to be planar such that their mechanical behavior is only governed by stress and strain components in the inclusion plan (x-y plan). The out-of-plane components are ignored here. It is assumed that the planar inclusion only has tensile behavior and its stress-strain relationship is described by a linear elastic-perfectly plastic constitutive model. In the case of plane strain analysis where the strain component perpendicular to the analysis plane (y-direction) is zero, the incremental form of stress-strain relationship is simplified to a one-directional form in terms of the x-direction stress component (σ_x^{inc}) and the corresponding strain direction (ε_x). The incremental stress-strain relationship has the following form [19]:

$$\dot{\sigma}_x^{inc} = D^{inc}\dot{\varepsilon}_x \tag{8}$$

where D^{inc} is the axial stiffness and $D^{inc} = E^{inc}/(1-\upsilon^{inc^2})$. E^{inc} and υ^{inc} are the elastic modulus and Poisson's ratio of the reinforcing inclusion.

Considering the Tresca yield criterion for the reinforcement phase with the tensile strength σ_{yield}^{inc}, the axial stress σ_x^{inc} is limited as follows [19]:

$$\sigma_x^{inc} \leqslant \frac{\sigma_{yield}^{inc}}{1-\upsilon^{inc^2}} \tag{9}$$

In the two-phase approach, the macroscopic characteristics of the reinforcement phase are introduced by the definition of volumetric reinforcement fraction (χ). According to Fig. 1, χ is defined in terms of inclusion thickness (t) and the distance between inclusions (h):

$$\chi = \frac{t}{h} \tag{10}$$

As a consequence, the macroscopic characteristics of the reinforcement phase are defined by:

$$\sigma_x^r = \chi\sigma_x^{inc}, \quad E^r = \chi E^{inc}, \quad \sigma_{yield}^r = \chi\sigma_{yield}^{inc} \tag{11}$$

The unit vector (**e**) parallel to the reinforcing layer is defined in terms of its inclination angle with respect to the horizontal (α) as follows:

$$\mathbf{e} = \{\cos\alpha, \sin\alpha\} \tag{12}$$

Thus, the stress and stiffness tensors of the reinforcement phase can be assessed:

$$\boldsymbol{\sigma}^r = \sigma^r(\mathbf{e} \otimes \mathbf{e}), \quad \mathbf{D}^r = D^r(\mathbf{e} \otimes \mathbf{e} \otimes \mathbf{e} \otimes \mathbf{e}) \tag{13}$$

where the symbol ⊗ denotes dyadic product of vectors.

2.2. Matrix phase behavior

In the reinforced soil medium, the volumetric portion of the soil against the inclusions (geosynthetic layers or steel bars for example) is very large and hence, the stress tensor of the matrix phase is assumed to be equal to that of the soil itself. Therefore, no modification is needed to transform the soil stress-strain relationship to that of the matrix phase.

In the present study, the behavior of the soil (and the matrix phase accordingly) is assumed to be linear elastic- perfectly plastic. The well-known Mohr-Coulomb failure criterion is adopted as the failure surface function (f) which is defined in terms of internal friction angle (ϕ) and cohesion (c) parameters as follows:

$$f(\boldsymbol{\sigma}) = \sigma_I - \sigma_{II} - \sin\phi(\sigma_I + \sigma_{II}) + c\cos\phi = 0 \tag{14}$$

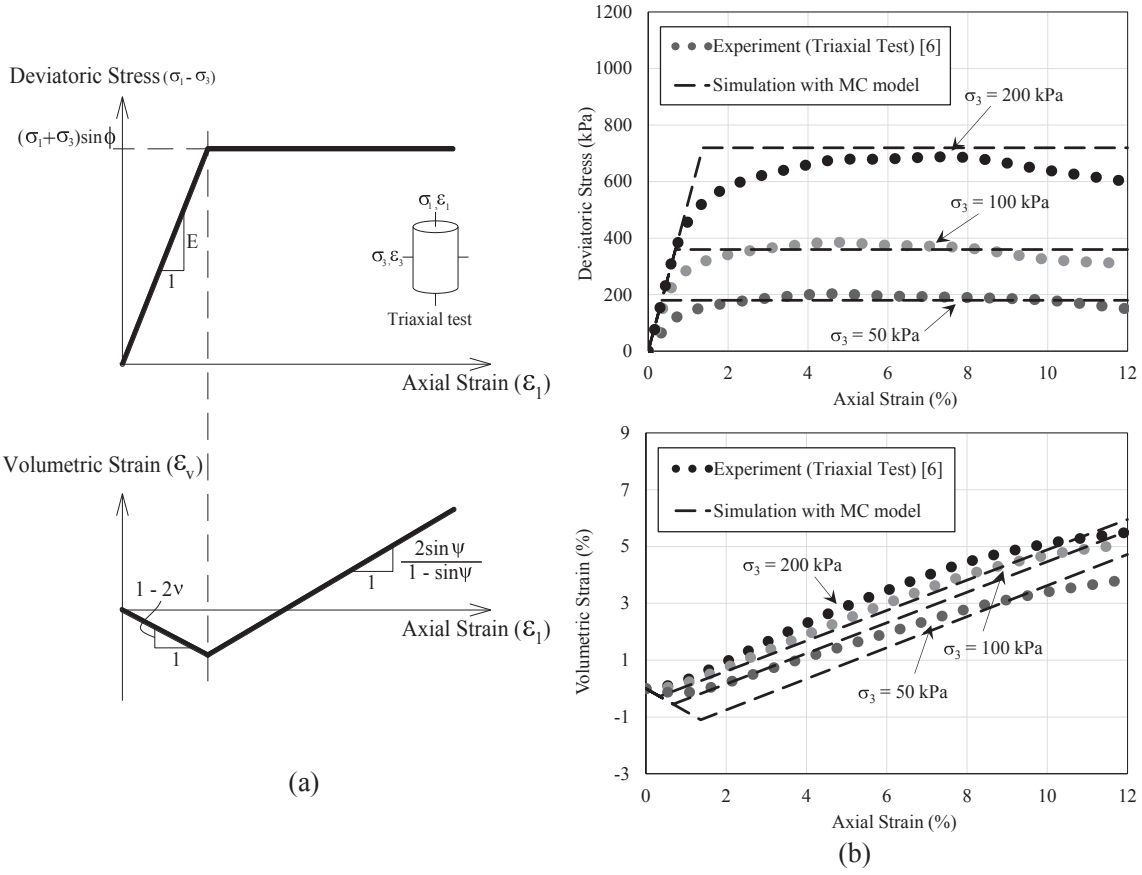

Fig. 3. Mechanical behavior of sandy soil in triaxial compression tests: (a) derivation procedure of elastic and plastic parameters; (b) comparison of experiment and simulations.

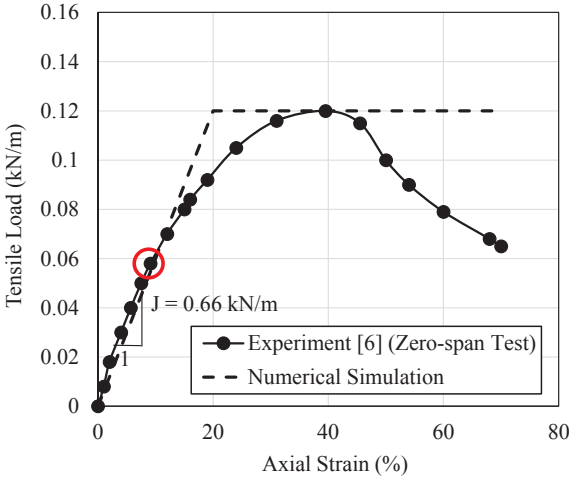

Fig. 4. Stress-strain relationship from experimental test and simulations using a linear elastic perfectly-plastic model.

where σ_I and σ_{II} are major and minor principal stress components. The incremental stress-strain relationship is defined as:

$$\dot{\boldsymbol{\sigma}}^m = \mathbf{D}^m(\dot{\boldsymbol{\varepsilon}}^m - \dot{\boldsymbol{\varepsilon}}^p) \tag{15}$$

The stiffness tensor $\mathbf{D}^m$ is defined in terms of the two parameters E (elastic modulus) and υ (Poisson's ratio). Based on the non-associated flow rule of incremental plasticity theory, the plastic strain increment ($\dot{\boldsymbol{\varepsilon}}^p$) is calculated by virtue of potential surface function (g):

$$\dot{\boldsymbol{\varepsilon}}^p = \langle \lambda^m \rangle \frac{\partial g}{\partial \boldsymbol{\sigma}} \tag{16}$$

where λ^m is the plastic loading multiplier. $\langle x \rangle = x$ for $x>0$ and $\langle x \rangle = 0$, otherwise. The potential surface function (g) is described by the dilatancy angle (ψ) parameter as follows:

$$g(\boldsymbol{\sigma}) = \sigma_I - \sigma_{II} + \sin\psi(\sigma_I + \sigma_{II}) \tag{17}$$

3. Numerical simulations

A series of experiential centrifuge tests on two-tier GRS walls are considered in this paper and the applicability of the two-phase model in predicting the mechanical behavior of such walls is investigated from the viewpoint of the interactions of the tiers with each other.

3.1. Centrifuge modeling

Centrifuge modeling is a useful technique in geotechnical engineering with which prototype structures can be studied as reduced scaled models while conserving the stress and strain states in the actual situation of the soil. Mohamed et al. [5] conducted a series of centrifuge modeling tests in order to investigate the performance and failure mechanisms of two-tier GRS walls. The details of centrifuge testing program have been reported by Hung [32] and only a brief description of the wall models and the test procedure are presented in this section.

A global scheme of two-tier GRS walls in centrifuge tests is depicted in Fig. 2. The heights of the upper (H_1) and lower (H_2) tiers are identical and $H_1 = H_2 = 160$ mm. An additional layer of 20 mm of soil is deposited on top of the upper tier to cover the topmost reinforcement layer, which results in a total height of H = 340 mm for all the walls.

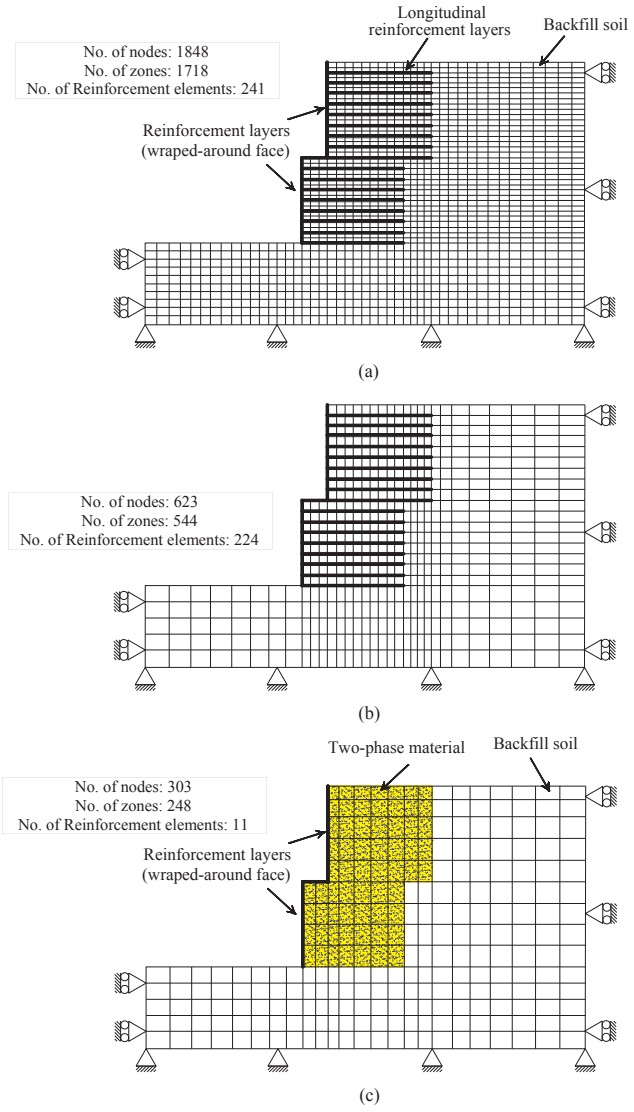

Fig. 5. Different grids used for the wall C6 in the numerical simulations: (a) fine grid for discrete model; (b) medium-sized grid for both discrete and two-phase model; (c) coarse grid for two-phase model. Dimensions are in accordance with the centrifuge models.

Table 2
Soil parameters of MC model used in the numerical simulations.

Density	Friction angle	Cohesion	Dilatancy angle	Elastic modulus	Poisson's ratio
γ (kN/m^3)	ϕ (degree)	c (kPa)	ψ (degree)	E (MPa)	ν (–)
15	42.3	1	12	66	0.25

Each wall is constructed on a 150 mm-thick layer of soil as foundation. The same number of reinforcement layers are used for all physical models, i.e. eight and nine layers for the lower and upper tiers, respectively with a 20 mm vertical spacing. Except for the topmost reinforcement layer, each reinforcement layer is folded back at the face of the wall models forming a wrap-around facing.

The wall models are categorized in three sets based on the offset distance between the upper and lower tiers as follows: (1) Single walls (S-series) in which two tiers constitute a single wall with similar upper (L_1) and lower (L_2) reinforcement lengths. Based on the FHWA recommendations, $L_1 = L_2 = 0.7$ and $H = 224$ mm was chosen; (2) Compound walls (C-series) in which the offset distance causes mutual interaction of the tiers. According to the FWHA design guideline, the offset distance (D) is in the range of H/20 and $H_2\tan(90^o-\phi)$, where ϕ the internal soil friction angle is. In these walls, $L_1 = L_2 = 0.6$ and $H = 192$ mm which meets the minimum length requirement ($L_1 = 0.7H_1$) according to FWHA in order to prevent instability of the upper tier; (3) Independent walls (I-series) where two tiers behave independently and no interaction exists between the tiers. According to the FHWA guideline, the offset distance (D) should be $D > H_2\tan(90^o-\phi)$ and $L_1 = L_2 = 0.7H_1 = 112$ mm. The geometrical characteristics of the walls considered in this study are depicted in Table 1.

Table 3
Parameters of reinforcing layers and reinforcement phases used in the numerical simulations.

Approach	Yield stress (kPa)	Elastic modulus (kPa)	Yield axial strain (%)	Poisson's ratio (–)
Discrete	120	660	18	0
Two-phase	6	33	18	0

Centrifuge modeling followed two stages. In the first stage, the wall model was spun to 40 g to compress any voids between the backfill soil and the reinforcement layers through increasing self-weight while the model was supported by a wooden formwork. The centrifuge was then decelerated to complete stop. In the second stage, the wooden formwork was removed and the models were loaded by gradually increasing their self-weight (by increasing the centrifuge acceleration) in 2 g increments. The weight was maintained for 30 s at each level of acceleration until the model failed. During the tests, the wall face deformation and failure mechanisms were recorded. The walls failed at elevated g-levels of 16 g (for S1) and 18 g (for C4, C6, C9, C10, I11), which correspond with the prototype wall heights of 5.5 and 6.1 m, respectively.

The failure mechanisms of the model walls were visually investigated at the end of the tests by focusing on the location of the torn reinforcement layers. The nearly-horizontal breakage pattern in the reinforcement layers showed that the plane strain condition was governing in the centrifuge tests. The location of the critical failure surface was determined based on the observed ruptures in each reinforcement layer.

3.2. Material properties

The soil used in the centrifuge tests was clean and uniform Fulung beach sand classified as poorly graded sand (SP) in the Unified Soil Classification System. The effective size (D_{10}) and average particle (D_{50}) size of the sand were 0.17 and 0.28 mm, respectively. The coefficient of uniformity and curvature of the sand were calculated to be 1.05 and 1.78, respectively. The backfill unit weight was obtained in the laboratory to be equal to $\gamma = 15$ kN/m^3. Triaxial compression tests were performed on the soil samples under three confining pressures of $\sigma_3 = 50$, 100, and 200 kPa in order to find the mechanical properties of the sandy soil.

The well-known Mohr-Coulomb (MC) model is adopted with the non-associated flow rule for the soil material as stated before. Application of the MC model provides a balance between simplicity, applicability, and prediction accuracy when used for simulating reinforced soil structures [33–36]. Fig. 3 shows the laboratory behavior of soil samples [6] in terms of variations of deviatoric stress and volumetric strain versus axial strain. The mechanical soil parameters of the MC constitutive model can be derived based on the simplified soil behavior using the MC model shown in Fig. 3a. The peak friction angle of the sand was obtained to be $\phi_{tx} = 39.5$ degrees. Regarding the elastic modulus (E) of the soil, the average secant slope corresponding to the

Fig. 6. Distribution of mobilized tensile loads for the wall C4 at the moment of failure (corresponding to the acceleration of 18 g) in terms of: (a) reinforcement phase stress; (b) axial loads along the reinforcement layers.

50% deviatoric stress - axial strain curve was derived to be E = 60 MPa. The Poisson's ratio (υ) of the sand was back calculated to be $\upsilon = 0.25$ from the initial slope of the volumetric strain versus axial strain. The dilation angle of the soil was estimated to be $\psi = 10^o$ from two approaches including an empirical equation proposed by Bolton [37] ($\psi = \phi - 30^o$) and the slope of the volumetric strain versus the axial strain at large strain level, as shown in Fig. 3a. The simulated mechanical behavior of the soil samples is sketched in Fig. 3b together with the experimental results.

The geotextile material used in the centrifuge tests was nonwoven polyester rayon fabric. A series of unconfined wide-width tensile tests [38] and zero-span tests [39] (under high confinement) were performed to evaluate the strength properties of the geotextile material. The average ultimate tensile load (T_{ult}) of the geotextile material was measured to be 0.05 kN/m from wide-width tests and 0.12 kN/m from zero-span tests. According to Mohamed et al. [5], the tensile behavior of the reinforcement layers are affected by soil confinement, and the response of the geotextile layer under zero span tensile test should be considered in the simulations.

Fig. 4 indicates the variations of axial load against axial strain of the nonwoven geotextile reinforcement under zero span test. The predicted load-strain curve is shown in the same Figure simulated by using the linear elastic perfectly-plastic model as explained in Section 2.1. The tensile stiffness of the reinforcement (J = 0.66 kN/m) is considered to be equal to the secant slope at 50% ultimate tensile strength (T_{ult} = 0.12 kN/m).

3.3. Numerical implementation

In order to numerically simulate the behavior of two-tier GRS walls, the commercial two-dimensional finite difference code FLAC is utilized in this study. In this study, the GRS two-tier walls are simulated by using discrete modeling approach as well as the two-tier approach. In the discrete modeling approach, the soil and reinforcement layers are individually considered in the numerical models.

The implementation of the two-phase formulation in the FLAC code was carried out by using the built-in language FISH. FLAC uses the explicit Lagrangian form of the finite difference method and the mixed-discretization zoning technique. Hence, the definition of stiffness or compliance matrices is not needed in the calculation scheme. The incremental form of stress – strain components of a two-phase material can be determined by using FISH. As a global scheme, incremental stress components are initially computed based on incremental total strain components by assuming elastic behavior for a two-phase material. Then, the stress components of each phase are evaluated. If they violate the corresponding yield criteria (Eqs. (9) and (14) for reinforcement and matrix phases, respectively), the stress components are corrected such that the stress point lies on the yield function of the corresponding phase. For the reinforcement phase, the one-component stress is simply controlled by using Eq. (9), while the correction of the stress components of the matrix phase is achievable by using its flow rule. In this case, only the elastic part of the strain increment components can contribute to the stress increment components (Eq. (15)). The elastic part is calculated by subtracting the plastic part from the total

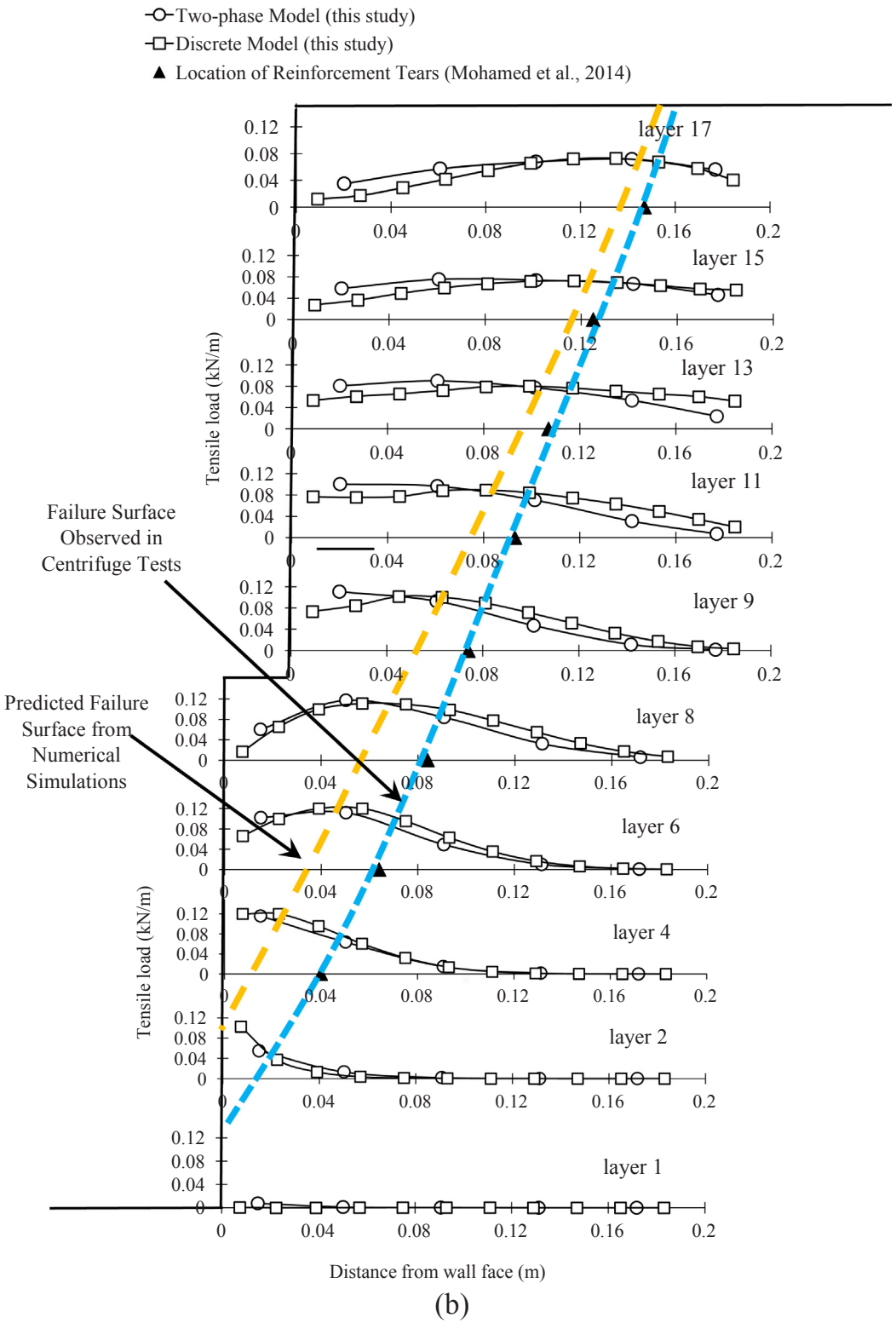

Fig. 6. (*continued*)

strain increment components. The plastic part is determined from the corresponding flow rule of the matrix phase (Eq. (16)).

For each wall configuration (refer to Table 1), a grid size study has been performed in order to find the effect of grid size on the accuracy of the results. For instance, three grid sizes as well as boundary conditions of wall C6 are depicted in Fig. 5. The same gird size has been taken into consideration for the other walls. The model dimensions are in accordance with those of the (centrifuge) model tests. Two fine and medium-sized grids were used for the numerical discrete approach, while the medium-sized and coarse grids were applied for the two-phase approach. The grid size of the reinforced soil in the two-phase model was intentionally chosen to be larger and almost equal to the backfill soil in order to examine the ability of the two-phase model to predict wall behavior. In the discrete models, the horizontal reinforcement layers on the back face of the wall as well as the vertical reinforcement layers are considered. In the two-phase models, only the

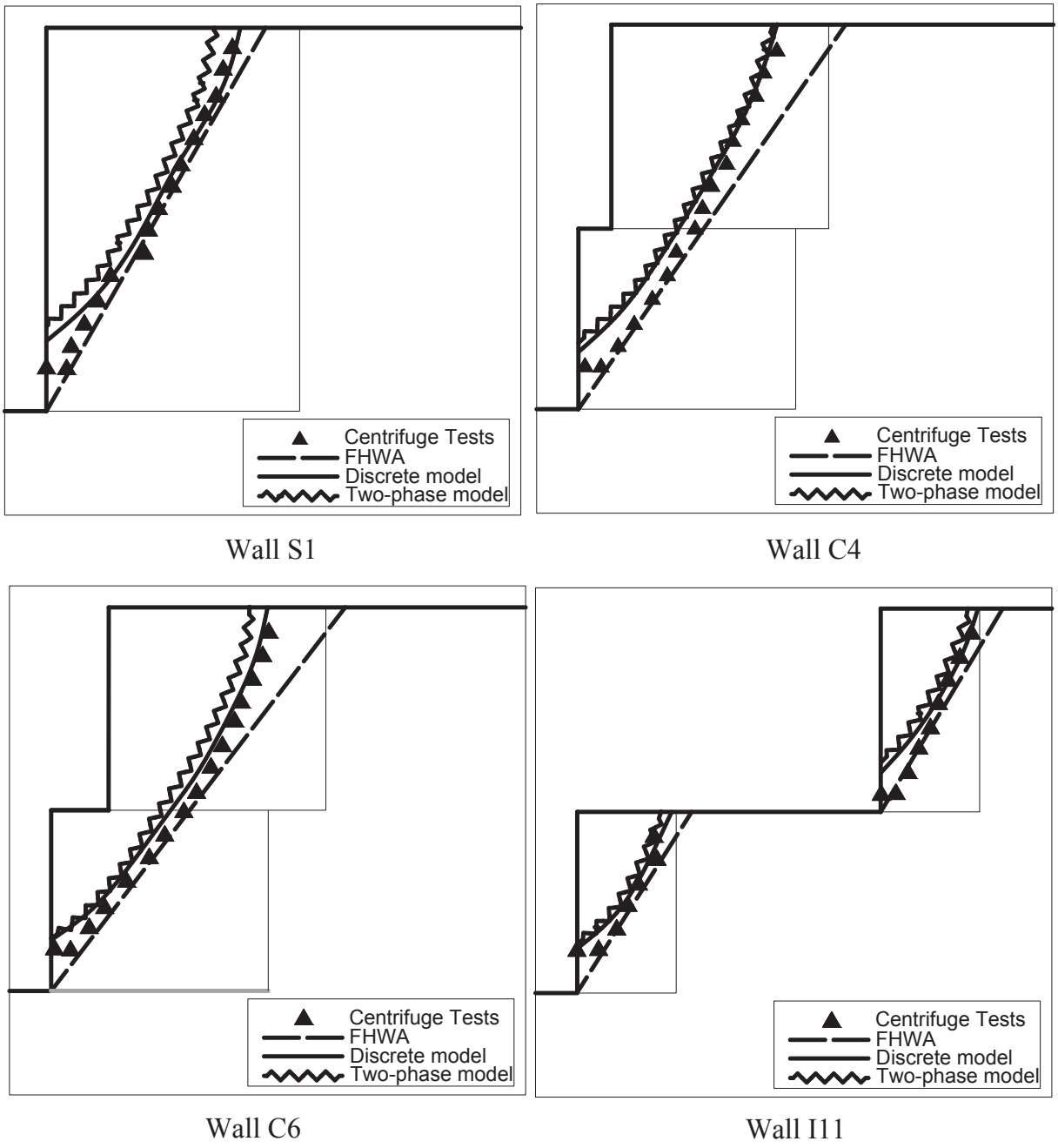

Fig. 7. Critical failure surface obtained from centrifuge tests and numerical simulations using discrete and two-phase models (based on maximum plastic strain increment).

vertical reinforcement layers are considered in order to model the wrapped-around wall face. The horizontal displacement of the sides of the models are fixed while the movement of both horizontal and vertical directions is fixed at the model's base.

The results of numerical simulations are compared with each other in terms of wall face deformation and reinforcement loads for all wall configurations. It is seen that for the discrete and two-phase approaches, medium-sized and coarse grids are, respectively, suitable for the analyses since they yield results similar to finer grids. Hence, the results presented in this study correspond to coarse and medium-sized grids for the two-phase and discrete models, respectively.

The physical models were made in centrifuge tests and physical tests were carried out under plane strain condition. Thus, soil parameters in the same conditions are required for plane strain numerical simulations. The peak plane strain friction angle of the soil is estimated using the correlation between triaxial compression friction angle (ϕ_{ts}) and plane strain friction angle (ϕ_{ps}) proposed by Lade [40] as $\phi_{ps} = 1.5\phi_{ts} - 17^{o}$. The dilation angle is corrected accordingly. The elastic modulus is modified by multiplying it by the ratio of tangent of plane strain friction angle to tangent of triaxial test friction angle ($\tan\phi_{ps}/\tan\phi_{ts} = 1.1$) as suggested by Mohamed et al. [6]. Since Poisson's ratio has a minor effect on the behavior, it is assumed not to be changed. The modified soil parameters are in accordance with Table 2 as used in the numerical simulations. It is also noted that in the numerical simulations, a small value was considered for soil cohesion (c = 1 kPa) in order to avoid soil instability in low confining pressures. It is reminded that these parameters are used for both the discrete and two-phase modeling approaches.

By considering a t = 1 mm thickness for the geotextile layer, the mechanical parameters of the numerical model are calculated. The elastic modulus is obtained from $E^{inc} = J/t$ and yield stress is

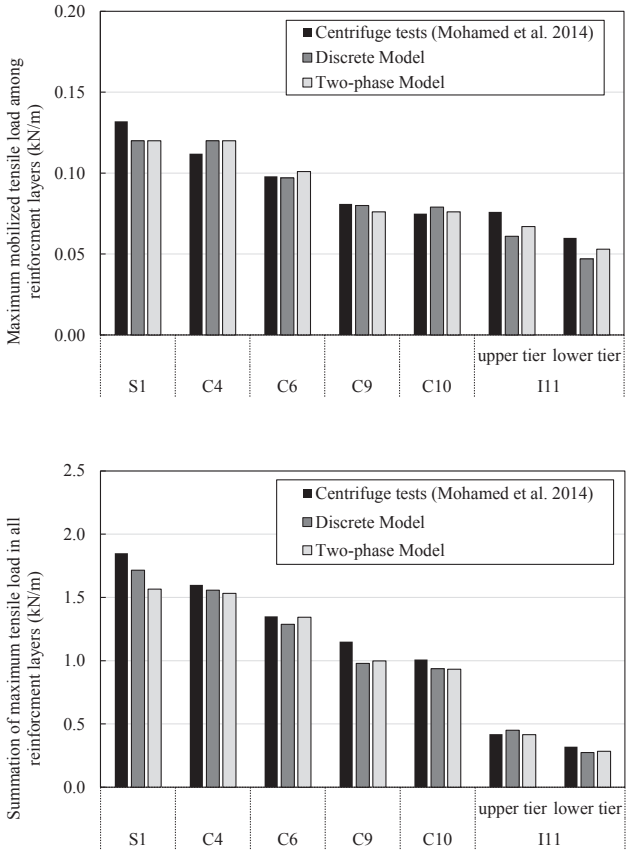

Fig. 8. Comparison of tensile load of reinforcement layers in different walls between centrifuge tests and numerical simulations.

$\sigma_{yield}^{inc} = T_{ult}/t$. According to Eq. (10), the volumetric reinforcement fraction is $\chi = 0.05$ and hence, the parameters of the reinforcement phase can be calculated by using Eq. (11). The parameters used in the numerical simulations are shown in Table 3.

In the numerical simulations, it is assumed that displacement compatibility exists between the soil and the reinforcement layers. This assumption is supported by the observations in the corresponding centrifuge tests [5] at the failure moment and in other experiments [41–45]. The same approach has been adopted in numerical studies where the soil in the corresponding experiment had a high degree of compaction and reinforcement pull out could not happen in the reinforced soil region [6,11,12,46,47]. Mohamed et al. [6] also reported that the primary failure of the models was because of reinforcement breakage rather than pullout. Accordingly, no interface is considered for the reinforcement layers in the discrete walls and the elements are attached to the soil grid. In the two-phase models, strain compatibility is assumed between the two phases which indicates perfect bonding condition as explained before in Section 2. It is clear that the application of the two-phase model in the form of perfect bonding should be prohibited for cases in which reinforcement layers are suspected to fail due to the pullout mechanism.

Numerical simulations of both groups (discrete and two-phase models) consist of two stages. In the first stage, the generated grids are brought into equilibrium under the gravity of 1 g where $g = 10\,m/s^2$. In this stage, geostatic stresses are generated inside the backfill soil. At the end, the grid displacements and strains are reset to zero since they are unreal in the model. In the second stage, the gravity magnitude in the models is increased by 2 g increments similar to the centrifuge tests. Then, the model is solved to reach the equilibrium state that corresponds to the condition when the maximum ratio of magnitude of unbalanced mechanical force divided by magnitude of applied mechanical force drops below 0.001 for all of the grid points in the model. The displacement of the wall face and axial stress/strains of the reinforcement layers are recorded at the end of each computational run. The increase in vertical acceleration continues until the measured failure g-level is reached.

4. Results and discussion

4.1. Failure surface

In conventional design approaches, the extent of failure surface in GRS walls is the determining factor in selecting an efficient length for reinforcement layers. In a safe design, the failure surface should pass through reinforcement layers indicating that the failure mechanism is governed by the reinforced soil region rather than the unimproved soil region. In the centrifuge tests, Mohammed et al. [6] determined the location of the critical failure surface based on visual inspection of tears in reinforcement layers. In numerical simulations, the failure surface can be found from the location of maximum mobilized tensile loads in reinforcement layers. Fig. 6 demonstrates the critical failure surface generated in wall C4 based on experiments and numerical simulations. Fig. 6a shows the distribution of axial stress in the reinforcement phase of the two-phase model. By considering the line passing through the maximum mobilized axial stress, the failure surface can be assessed. The highlighted triangles represent the location of the reinforcement tiers observed in the centrifuge test. By comparing the experimental and numerical results, it can be found that the critical failure surface from the two-phase model is predicted slightly in front of the actual failure surface (observed in the centrifuge test). Fig. 6b shows the predicted mobilized tensile loads along the length of the reinforcement layers for wall C4 based on both discrete and two-phase numerical models. In the discrete model, the mobilized axial force along the reinforcements is obtained directly. However, the distribution of axial force in the reinforced zone in the two-phase model can be obtained from the reinforcement phase stress distribution as already depicted in Fig. 6a. In this model, the axial tensile load of the reinforcement layers can be obtained by recording the value of the reinforcement phase stress along the lines passing from the location of the layers. Comparison of axial loads of the reinforcements from the two models shows a good agreement both in trend and value. The location of rupture of each reinforcement that is observed in the centrifuge test is also depicted in the same Figure. In addition to the coincidence of the loci of predicted failure surfaces, it can be seen that, the failure surfaces from numerical analyses are generated in front of the failure surface observed in the test similar to Fig. 6a.

In numerical simulations, the critical failure surface can also be recognized by finding the loci of maximum shear strain increments in the medium. In Fig. 7, the failure surface of four GRS walls including walls S1 (single), C4, C6 (compound two-tier) and I11 (independent two-tier) are depicted based on the experiment, conventional approach according to the FHWA guideline, and the two numerical simulation approaches (discrete and two-phase models). In all parts of Fig. 7, it can be seen that the maximum tension line (dash line) suggested by the FHWA guideline passes through the wall toe while no rupture was found in the first reinforcement layer in the centrifuge tests. Therefore, the actual failure surface was created at the upper layer. According to Mohammed et al. [6], the FHWA failure surface can predict the actual failure surface of single wall (S1) and independent tier walls (I11) well. However, it would give overestimation of required reinforcement lengths for compound walls. Considering the results of numerical simulations, there is an overall good agreement between the predicted failure surface obtained from the discrete model and that of the centrifuge tests. The failure surface assessed from the two-phase model is generated slightly in front of that of the discrete model. It is noteworthy that the results reported here are related to the coarse grid. An extra investigation on grid size indicates that the predicted surface from the two-phase model coincides with that of the discrete model if the same

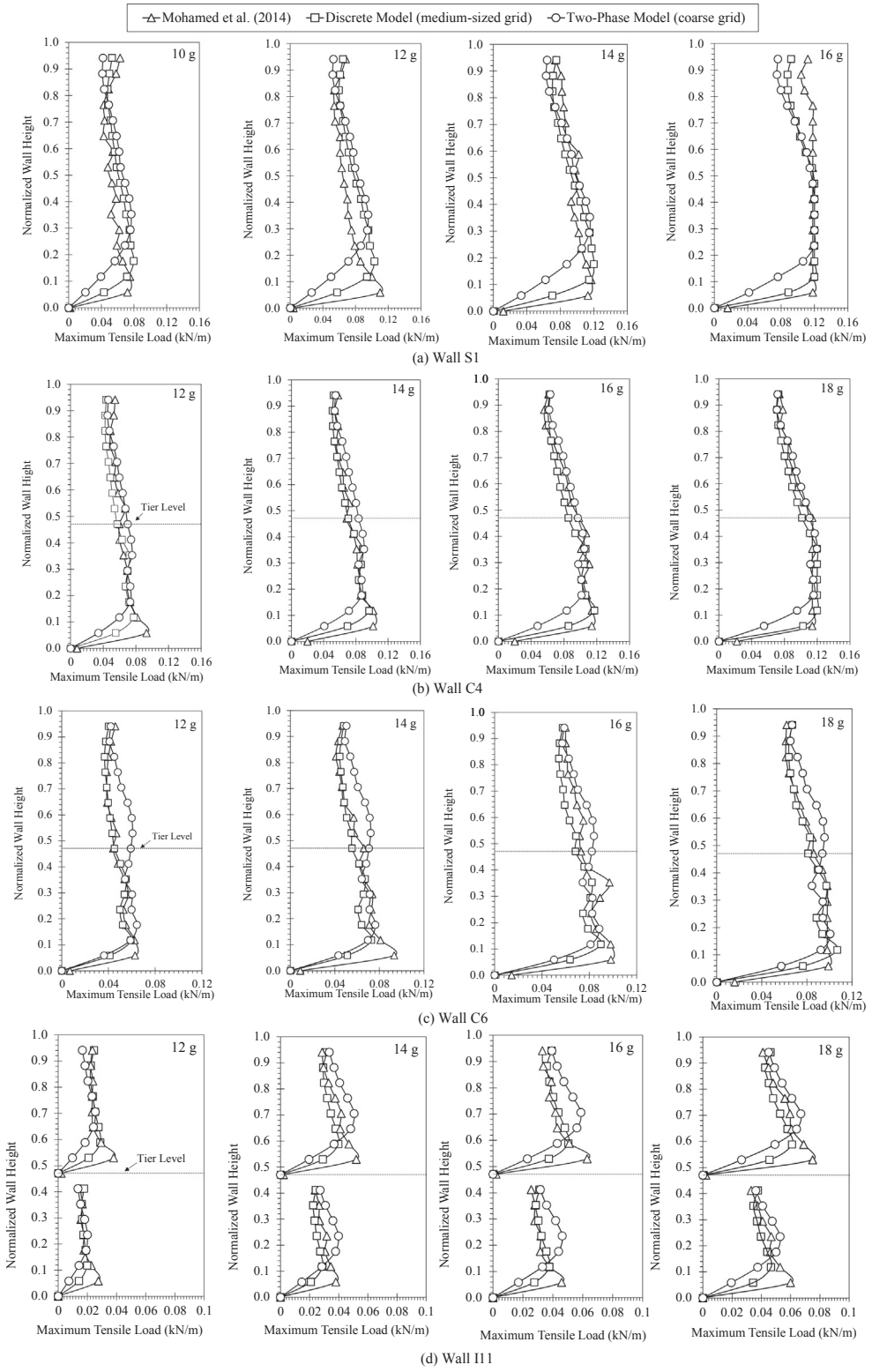

Fig. 9. Distribution of maximum tensile load with normalized wall height obtained from different approaches.

grid size is applied in the numerical model.

Generally, there is a good agreement between the failure surfaces obtained from simulations and those from centrifuge tests. The similarity is much better in the upper parts of the walls. However, it reduces in deeper layers especially around the wall toe where the failure surface crosses the wall face. This non-coincidence might be attributed to the limitation of the soil constitutive model since the soil parameters like stiffness in the MC model are not sensitive to stress variations with depth. Thus, a good distribution of plastic strains in the soil medium is not considered well. It is noted that the failure surfaces of the walls derived based on the numerical finite element (FE) simulations performed by Mohamed et al. [6] show a better agreement since a hardening soil model was implemented in the simulations in which soil stiffness increased with increased depth. It should be noted that the

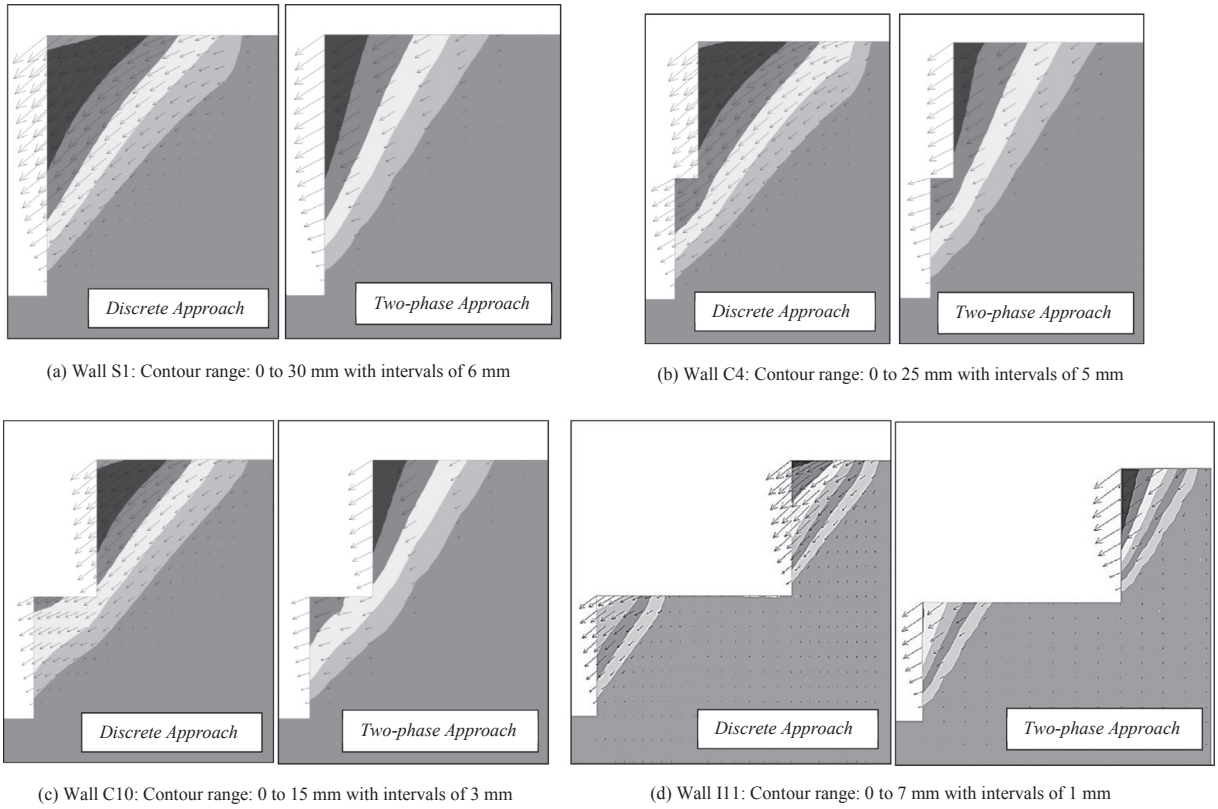

(a) Wall S1: Contour range: 0 to 30 mm with intervals of 6 mm

(b) Wall C4: Contour range: 0 to 25 mm with intervals of 5 mm

(c) Wall C10: Contour range: 0 to 15 mm with intervals of 3 mm

(d) Wall I11: Contour range: 0 to 7 mm with intervals of 1 mm

Fig. 10. Contours of walls horizontal deformation as well as displacement vectors obtained from numerical simulations using discrete and two-phase approaches at the failure moment (failure acceleration levels).

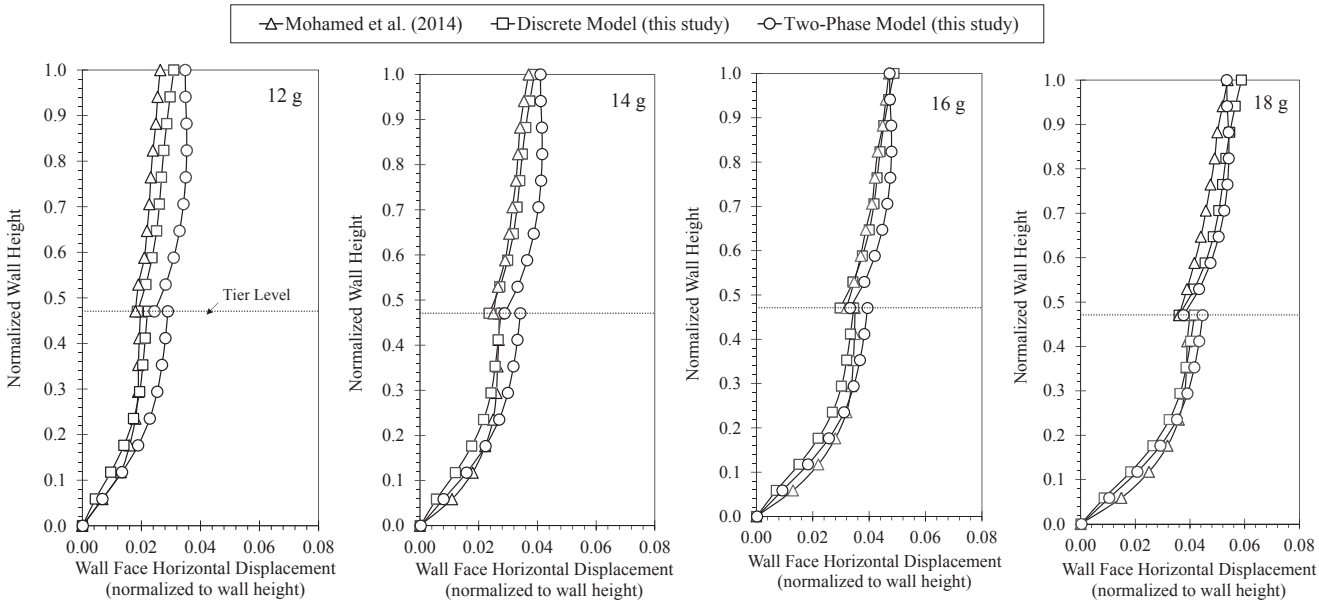

Fig. 11. Presentation of horizontal displacement of the wall C6 face along wall height from different approaches.

main objective of application of numerical modeling is not to find the critical failure surface. Rather, the main objective of using numerical simulations is to find the distribution of reinforcement loads and wall deformation.

4.2. Reinforcement loads

In order to investigate the applicability of numerical simulations in predicting reinforcement loads, the maximum tensile loads mobilized in the reinforcements of the walls are compared. A comparison of results from the centrifuge tests (back-calculated from LE method) and those obtained from both discrete and two-phase numerical models are shown in Fig. 8. The values of the maximum tensile load in each wall and the summation of all maximum tensile loads mobilized in all of the walls are depicted in Fig. 8a and b, respectively. A good agreement exists between the results of the experimental tests and those of numerical simulations in general. The predicted values obtained from the simulations are slightly smaller than those of the experiment, and this

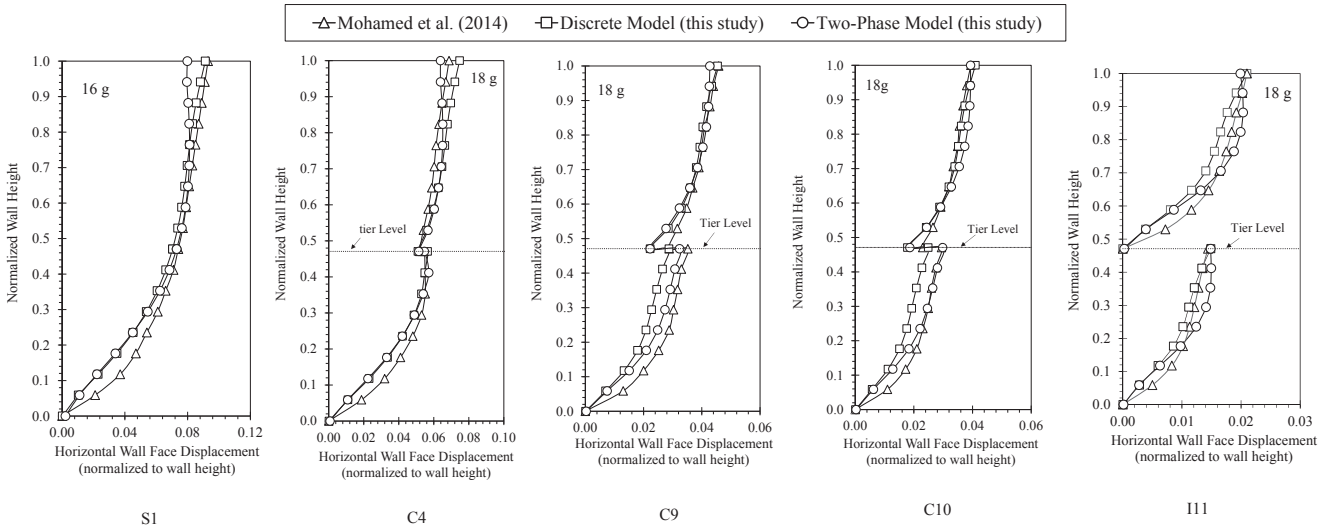

Fig. 12. Variation of horizontal wall face displacement along the wall height for different walls at the moment of failure.

difference is negligible. The general trend observed in the magnitude of loads indicates that the maximum load is the highest in the single wall (S1), but it decreases as the offset distance between the two tiers increases. In this Figure, the value of the maximum loads mobilized in the upper and lower tiers of the wall I11 are shown separately. This indicates a big reduction in reinforcement loads. The reason for this is the large distance between the tiers such that two walls with smaller height have the least interaction and thus behave independently.

In order to investigate the ability of the two-phase model in simulating the reinforcement load distribution along the wall height, the variation of maximum reinforcement loads from numerical simulations for the four S1, C4, C6, and I11 walls are presented in Fig. 9 along with the FE results performed by Mohamed et al. [6], validated based on the centrifuge tests results. Comparison of the graphs indicates that the numerical results of this study agree well with that of the experiment except for the lower tier close to the wall toe, where the predicted tensile load from the two-phase model is smaller. This imperfection corresponds with the weak prediction of the failure surface around the toe which was generated slightly in front of the actual surface as discussed before. Nevertheless, this discrepancy only exists in less than 10% of the total height and does not seems to be of concern.

4.3. Wall face displacement

The performance of a GRS wall is determined by wall deformation under loading conditions. Thus, a good prediction of wall displacement is an important parameter that indicates the efficiency of numerical analyses. The deformation patterns of walls S1, C4, C10, and I11 are plotted in Fig. 10 from the numerical simulations using both discrete and two-phase approaches. The results correspond to the acceleration levels where wall failure had occurred, i.e., at 16 g for wall S1 and 18 g for the rest of the walls. Moreover, the total displacement vectors are depicted for a better perception. By comparing the results for each couple, it can be seen that the global deformation patterns are very similar. The extent of deformation behind the walls is found to be slightly larger for the discrete model due to the finer grid used for the discrete model. Furthermore, by comparing the wall types, it can be seen that the magnitude of wall deformation is attenuated as the offset distance increases. No data about the deformational pattern behind the wall face is reported in the reference paper. In this section, the results of numerical simulations are compared with experimental results in terms of wall face displacement which was also measured in different loading stages.

Fig. 11 presents the horizontal displacement of the face of wall C6 under several levels of accelerations, i.e. 12 g, 14 g, 16 g, and 18 g. It can be seen that the results of using the discrete model agree well with the predictions of Mohamed et al. [6] for all acceleration levels while wall face displacement is slightly overestimated for small and middle g-levels (12 g and 14 g) when using the two-phase model. However, this discrepancy disappears as acceleration level increases and the results agree with each other.

The horizontal face displacement of walls S1, C4, C9, C10, and I11 along the wall height at the corresponding failure acceleration levels is depicted in Fig. 12 in order to investigate the efficiency of numerical simulations for different wall configurations. Although the wall face is slightly under-predicted by the discrete model for compound walls C9 and C10 for lower tiers, it can be generally seen that the results of both discrete and two-phase models agree well with the results reported by Mohamed et al. [6].

4.4. The effect of offset distance

The offset distance between the two tiers plays an important role in the mechanical behavior of two-tier walls. In order for to investigate the effect of offset distance on walls deformation, the horizontal displacement of all of the walls are sketched altogether in Fig. 13 for both discrete and two-phase models. Totally, the same trend in wall face deformation can be seen with respect to the effect of offset distance in both groups of simulations. Wall deformation is the largest for a single wall and it decreases as offset distance increases. For an independent wall (I11), deformation at the toe of the upper tier gets zero. Therefore, the lower tier has no effect on the deformation of the upper one. Although both groups of simulations can efficiently consider the effects of offset distance, it can be found that the wall face deformation pattern for the upper tier is somehow different in the two-phase model in comparison with the discrete model. A cantilever-type pattern is recognized for wall face deformation when the discrete approach is applied, but in the two-phase model, the lateral movement at the top of the upper tier is found to be slightly smaller with respect to the lower levels. As a result, the deformational pattern of the wall face seems to be nearly of the bulge-like type. A grid size study shows that the deformational pattern is not changed even when a finer grid size is considered in the two-phase model. Nevertheless, by referring to Fig. 12, it can be seen that the difference in the magnitude of the lateral movement between the two approaches is negligible.

It is now obvious that the offset distance between the two tiers can

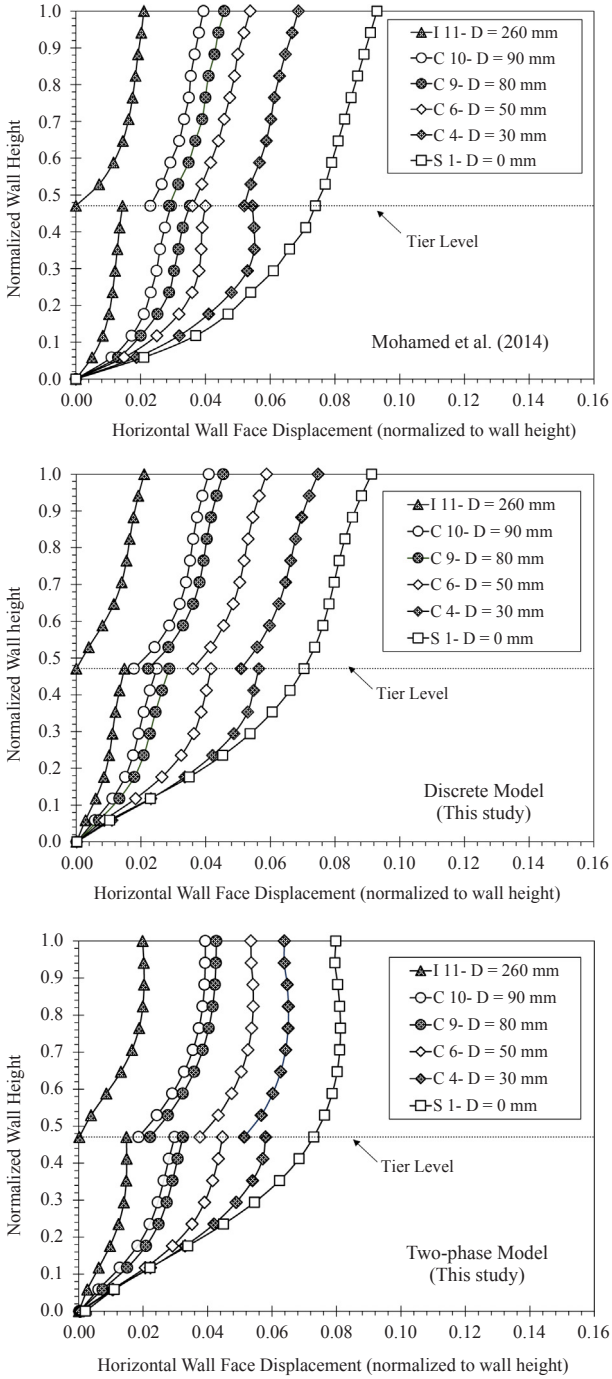

Fig. 13. Schematics of wall face deformation patterns for different offset distances.

influence the mechanical behavior of two-tier GRS walls including the deformational regime as well as the distribution of reinforcement loads. The interaction between the tiers is due to the equivalent surcharge of the upper tier over the lower one. The critical offset distance (D_{cr}) is defined as the offset distance at which the two tiers have no mutual effects. In the literature, the critical offset distance has been determined based on the impressionability of either reinforcement loads by using LE/numerical analyses [4,5] or lateral displacement of the wall face [6,8] at the moment of failure by applying numerical simulations.

Fig. 14 presents the scattering of the maximum tensile load mobilized in the reinforcement layers and the maximum lateral displacement against the normalized offset distance with respect to the upper tier height (D/H_2) at the moment of wall failure. The results are separately shown for the upper and lower tiers of the walls. As seen, the values of reinforcement and lateral displacement decrease as the offset distance increases. The trends observed in the results obtained from both groups of two-phase and discrete models are similar. In addition, the same similarity exists between the graphs based on reinforcement loads and wall lateral displacement. It can be seen that for the individual upper and lower tiers, there is almost a linear relationship for the results of single and compound walls and this decreasing trend can be approximated by a line. Since the tiers of the wall I11 have independent behaviors, one horizontal line is considered passing through the point. The critical offset distance is estimated by intersecting these two lines and choosing the biggest intersection value between the upper and lower tiers, Application of discrete numerical analysis yields $D_{cr} = 0.80H_2$ based on the maximum reinforcement load analysis and $D_{cr} = 0.77H_2$ if the wall face displacement is considered. By using the two-phase approach, $D_{cr} = 0.71H_2$ and $D_{cr} = 0.80H_2$ are extracted based on the maximum reinforcement load and the wall face lateral movement criteria, respectively.

The normalized values of critical offset distance with respect to the lower tier height (D_{cr}/H_2) obtained from different approaches are reported in Table 4. The results are categorized on either the basis of reinforcement load or wall face displacement. Other studies that have been done using the LE/FE methods have reported the ratio of D_{cr}/H_2 to be in the range of 0.7–0.8 and the results of this study are in good agreement with this. Meanwhile, the D_{cr} value gives $D_{cr} = 1.1H_2$ by assuming $\phi = 42.3^{\circ}$ based on the FHWA guideline design method. This value is estimated to be higher than the results reported in other studies since the upper tier is considered to be a single wall and its interaction with the lower tier has been ignored in the empirical method suggested by FHWA.

5. Concluding remarks

The numerical simulations of a series of centrifuge modeling of two-tier Geosynthetic Reinforced Soil (GRS) walls are presented in this study. For the numerical analyses, two different approaches including the discrete and two-phase modeling techniques were implemented and the applicability of the two-phase approach was investigated in comparison with the discrete modeling approach. In the discrete model, the soil and the reinforcement layers are separately considered in the numerical model. In the two-phase model, the reinforced soil region is replaced by a two-phase material. Comparison of the results of numerical and experimental models indicates the following:

- The grid size used in the numerical two-phase model can be coarser than that of the discrete model giving the same results in terms of wall deformation and reinforcement load distribution. It is clear that the expense of numerical modeling would reduce as the grid size increases.
- The critical failure surface obtained from the discrete model agrees well with the experiment. The grid size used for the two-phase model can influence the predicted failure surface. In the case of coarser grid size in the two-phase model compared with the discrete model, the failure surface is predicted slightly in front of the actual failure surface. The grid size equal to the discrete model would yield the same results.
- The failure surface obtained from the numerical simulation can be determined from the loci of either maximum plastic strain increment or maximum mobilized reinforcement load. The latter can be more easily recognized from the distribution of axial stress in the reinforcement phase when using the two-phase model.
- Contrary to the failure surface, the wall face displacement and the mobilized reinforcement load are not sensitive to grid size when using the two-phase model. It is noted that in the design of GRS walls, performance is evaluated by the wall face deformation and the reinforcement loads rather than the failure surface.

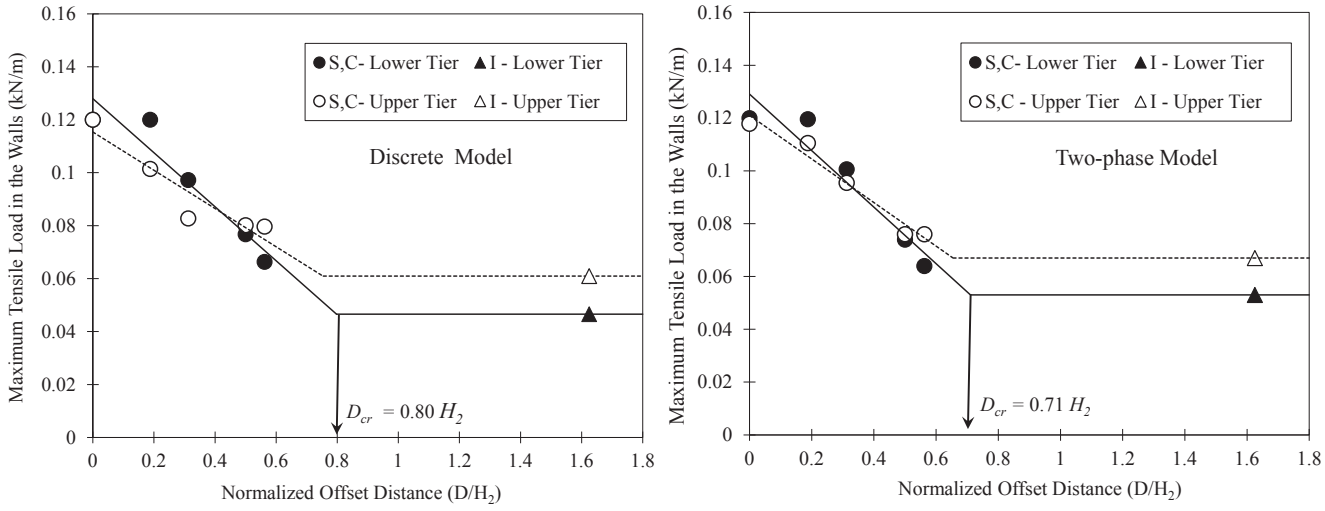

(a) Based on reinforcement load

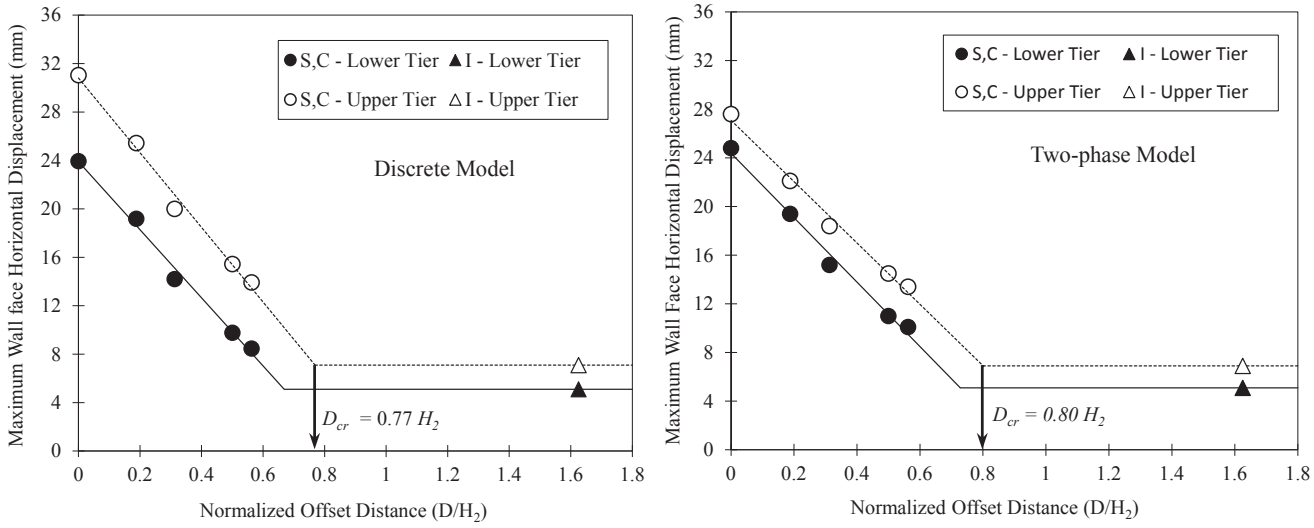

(b) Based on wall face deformation

Fig. 14. Determination of critical offset distance (D_{cr}) from numerical simulations performed in this study.

Table 4
Comparison of D_{cr}/H_2 values obtained from different approaches.

Approach	Criterion based on		Reference
	Reinforcement loads	Wall displacement	
Experimental	$\tan(90^\circ-\phi) = 1.1$		FHWA (Berg et al. [2]; Elias et al. [3])
Limit equilibrium	0.8	–	Leshchinsky and Han [4]
	0.7	–	Mohamed et al. [5]
Numerical simulation	–	0.8	Yoo et al. [8]
	0.73	0.82	Mohamed et al. [6]
	0.8	0.77	This study (Discrete model)
	0.77	0.8	This study (Two-phase model)

- A good agreement exists between the discrete and two-phase models for variations of maximum mobilized tensile load in the reinforcement layers along the height of the wall.
- The deformational pattern of the wall face for the upper tier was predicted to be cantilever-type in the discrete model while a bulging pattern was observed in the two-phase model.
- The two-phase model can consider the mutual interaction of the tiers. Based on the reinforcement load and the wall face deformation, the critical offset distance beyond which the two tiers behave independently is estimated to be in the range of D_{cr} = 0.7–0.8H_2, that agrees well with the results of other research reports based on LE and numerical analyses.

Based on the results mentioned above, it can be concluded that the two-phase model can be applied in the design and analysis of two-tier walls especially when it is desired to assess reinforcement load distribution and mobilized magnitudes. The wall face deformation can give a good estimation. However, the deformation pattern might not be accurately predicted. Furthermore, the mutual interaction between the tiers can be studied with an acceptable degree of accuracy. The two-phase model may not be reliable for finding the failure surface at the moment of wall failure since it would be generated slightly in front of the actual failure surface.

The present work only focused on the predictions of the two-tier GRS walls by applying simple constitutive models of the soil and

reinforcement layer materials in the framework of two-phase approach. In order to improve the accuracy of predictions, advanced constitutive models can be implemented in the numerical simulations which is also applicable in the framework of the two-phase approach. It is also noted that the present form of the two-phase model (with perfect bonding condition) is only applicable to the analysis of reinforced soil walls where the pullout of the layers is not dominant and does not occur. Otherwise, the analysis would lead to aberrant results.

Acknowledgement

The authors gratefully acknowledge the financial support granted by the Research Deputy of the Ferdowsi University of Mashhad with project no. 2-42353-11-10-1395.

References

[1] NCMA. Design manual for segmental retaining walls. 3rd ed. Herndom, Virginia, USA: National Concrete Mansory Association; 2010. p. 282.
[2] Berg R, Christopher BR, Samtani N. Design of mechanically stabilized earth walls and reinforced soil slopes report No. FHWA-NHI-10-024,25; 2009. < https://www.fhwa.dot.gov/engineering/geotech/pubs/nhi10024/ > .
[3] Elias V, Christopher BR, Berg R. Mechanically stabilized earth walls and reinforced soil slopes design and counstruction guidelines. Federal Highway Administration; 2001.
[4] Leshchinsky D, Han J. Geosynthetic reinforced multi-tiered walls. Geotech Geoenviron Eng ASCE 2004;130(12):35–1225.
[5] Mohamed SBA, Yang K-H, Hung W-Y. Limit equilibrium analyses of geosynthetic-reinforced two-tiered walls: Calibration from centrifuge tests. Geotext Geomembr 2013;41:1–16.
[6] Mohamed SBA, Yang K-H, Hung W-Y. Finite element analyses of two-tier geosynthetic -reinforced soil walls: comparison involving centrifuge tests and limit equilibrium results. Comput Geotech 2014;61:67–84.
[7] Rahmouni O, Mabrouki D, Benmeddour D, Mellas M. A numerical investigation into the behavior of geosynthetic-reinforced soil segmental retaining walls. Int J Geotech Eng 2016;10(5):435–44.
[8] Yoo C, Jang YS, Park IJ. Internal stability of geosynthetic-reinforced soil walls in tiered configuration. Geosynth Int 2011;18(2):74–83.
[9] Stuedlein AW, Bailey M, Lindquist D, Sankey J, Neely WJ. Design and performance of a 46-m-high MSE wall. J Geotech Geoenviron Eng 2010;136(6):86–96.
[10] Wright SG. Design guidelines for multi-tiered MSE walls. Austin, Texas: FHWA/TX-05/0-4485-2; 2005.
[11] Yoo C, Song AR. Effect of foundation yielding on performance of two-tier geosynthetic reinforced segmental retaining walls: a numerical investigation. Geosynth Int 2007;20(3):20–110.
[12] Yoo C, Kim SB. Performance of a two-tier geosynthetic reinforced segmental retaining wall under a surcharge load: full-scale load test and 3D finite element analysis. Geotext Geomembr 2008.
[13] de Buhan P. Yield design of reinforced earth walls by a homogenization method. Géotechnique 1989;39:189–201.
[14] Harrison WJ, Gerrard CM. Elastic theory applied to reinforced earth. J Soil Mech Foundations Division ASCE 1972;98(12):1325–45.
[15] Herrmann L, Welch K, Lim C. Composite FEM analysis for layered systems. J Eng Mech 1984;110(9):1284–302.
[16] Michalowski RL, Zhao A. Continuum versus structural approach to stability of reinforced soil. J Geotech Eng Division ASCE 1995;121:152–62.
[17] de Buhan P, Sudret B. A two-phase elastoplastic model for uni-directionallyreinforced materials. Eur J Mech A/Solids 1999;18:995–1012.
[18] Ben Hassine W, Hassis H, de Buhan P. A macroscopic model for materials reinforced by flexible membranes. Mech Res Commun 2008;35(5):310–9.
[19] Seyedi Hosseininia E, Farzaneh O. Development and validation of a two-phase model for reinforced soil by considering nonlinear behavior of matrix. J Eng Mech 2010;136(6):721–35.
[20] Seyedi Hosseininia E, Farzaneh O. A simplified two-phase macroscopic model for reinforced soils. Geotext Geomembr 2010;28:85–92.
[21] Honari S, Seyedi Hosseininia E. Numerical modeling of reinforced soil walls using multiphase approach and hyperbolic constitutive model. J Ferdowsi Civil Eng 2016;28(1):81–98.
[22] Farzaneh O, Iraji A. Two-phase model for nonlinear dynamic simulation of reinforced soil walls based on a modified pastor-zienkiewicz-chan model for granular soil. Eng Mech 2016;142(2).
[23] Sudret B, de Buhan P. Multiphase model for inclusion - reinforced geostructures: Application to rock-bolted tunnels and piled raft foundations. Int J Numer Anal Methods Geomech 2001;25(2):155–82.
[24] de Buhan P, Bourgeois E, Hassen G. Numerical simulation of bolt supported tunnels by means of a multiphase model conceived as an improved homogenization procedure. Int J Numer Anal Meth Geomech 2008;32:1597–615.
[25] Hassen G, de Buhan P. Elastoplastic multiphase model for simulating the response of piled raft foundations subject to combined loadings. Int J Numer Anal Meth Geomech 2006;30:843–64.
[26] Bennis M, de Buhan P. A multiphase constitutive model of reinforced soils accounting for soil-inclusion interaction behaviour. Math Comput Modell 2003;37(5–6):469–75.
[27] Nguyen VT, Hassen G, de Buhan P. A multiphase apprach for evaluating the orizontal and rocking impedence of pile group foundations. Int J Numer Anal Meth Geomech 2016;40:1457–71.
[28] Thai Son Q, Hassen G, de Buhan P. Seismic stability analysis of piled embakements: A multiphase approach. Int J Numer Anal Meth Geomech 2010;34:91–110.
[29] Sudret B. Modelisation multiphasique des ouvrages reforces par inclusions. Paris; 1999.
[30] Thai Son Q, Hassen G, de Buhan P. A multiphase approach to the stability analysis of reinforced earth structures accounting for a soil-strip failure condition. Comput Geotech 2009;36:454–62.
[31] Bourgeois E, Hassen G, de Buhan P. Finite element simulations of the behavior of piled-raft foundations using a multiphase model. Int J Numer Anal Meth Geomech 2012;37:1122–39.
[32] Hung WY. Breaking failure behavior and internal stability analysis of geosynthetic reinforced earth walls. Jhongli, Taiwan: National Central University; 2008.
[33] Huang B, Bathurst RJ, Hatami K. Numerical study of reinforced soil segmental walls using three different constitutive models. J Geotech Geoenviron Eng 2009;2009(135):10.
[34] Seyedi Hosseininia E. A comparative numerical study of a geosyntheticreinforced soil wall using three different constitutive soil models. Iranian J Sci Technol, Trans Civil Eng 2015;39(C1):125–41.
[35] Hatami K, Bathurst RJ. Development and verification of a numerical model for tha analysis of geosynthetic reinforced soil segmental walls working stress conditions. Can Geotech J 2005;42(4):1066–85.
[36] Holtz RD, Lee WF. Internal stability analysis of geosynthetic reinforced retaining walls. Technical report for Washington State Transportation Commision, vol. 466; 2002.
[37] Bolton MD. The strenght and dilatancy of sands. Geotechnique 1986;36(1):65–78.
[38] D4595 A. Standard test method for tensile properties of geotextiles by the wide-width strip method, vol. 4.09. West Conshohocken, PA: Annual Book of ASTM Standardsm; 1996. p. 698–708.
[39] Porbaha A, Goodings DJ. Centrifuge modeling of geotextile reinforced cohesive soil retaining walls. J Geotech Eng Division ASCE 1996;122(10):840–8.
[40] Lade P, Lee K. Engineering properties of soils. Loas Angeles: University of California; 1976. p. 145.
[41] Palmeira EM. Soil-geosynthetic interaction: modeling and analysis. Geotext Geomembr 2009;27(5):368–90.
[42] Ferreira FB, Vieira CS, Lopes ML. Direct shear behavior of residual soilgeosynthetic interfaces-influence of soil moisture content, soil density and geosynthetic type. Geosynthetics Int 2015;22(3):257–72.
[43] Lopes ML. Soil-geosynthetic interaction. In: Shukla SK, editor. Handbook of geosynthetic engineering. London: ICE Publishing; 2012. p. 45–66.
[44] Vieira CS, Lopes ML, Calderia LM. Sand-geotextile interface characterization through monotonic and cyclic direct shear tests. Geosynthetics Int 2013;20(1):26–38.
[45] Afzali-Nejad A, Lashkari A, Tabatabaie Shourijeh P. Influence of particle shape on the shear strength and dilation of sand-woven geotextile interfaces. Geotext Geomembr 2017;45(1):54–66.
[46] Zorenberg JG, Arriaga F. Strain distribution within geosynthetic-reinforced slopes. J Geotech Geoenviron Eng 2003;129(1):32–45.
[47] Zorenberg JG, Sitar N, Mitchell JK. Performance of geosynthetic reinforced slopes at failure. Geotech Geoenviron Eng 1998;124:670–83.